Design, Modelling and Control Implementation of PV-MPPT Based DC-DC Converter for STATCOM

IOP Conf. Series: Materials Science and Engineering **495** (2019) 012035 doi:10.1088/1757-899X/495/1/012035

Design, Modelling and Control Implementation of PV-MPPT Based DC-DC Converter for STATCOM

K H Law[1], W P Q Ng[2] and P I Au[3]
[1] Department of Electrical and Computer Engineering, Curtin University, CDT 250, Miri 98009, Sarawak, Malaysia
[2] Department of Chemical Engineering, Curtin University, CDT 250, Miri 98009, Sarawak, Malaysia
[3] Department of Chemical Engineering, Curtin University, CDT 250, Miri 98009, Sarawak, Malaysia

Abstract. In spurring towards a lower-carbon and renewable energy dependent future, this paper considered the requirements of the Malaysian climate and transmission network in designing a system that extracts maximum power from photovoltaic (PV) and provides AC source-side reactive power compensation. In modelling a system appropriate for energy demands of Malaysia, solar irradiance is varied from 1.25 kW/m^2 to 5 kW/m^2 and temperature between 25°C and 50°C. An average simulation model is first designed, incorporating the control elements demonstrated by the selected maximum power point tracking (MPPT) algorithm and static synchronous compensator (STATCOM) control scheme for balanced loading conditions. To justify the results obtained, a second detailed model is designed to account for inclusion of harmonics. Power factor of 0.8 was employed for the average and detailed models before the providence of reactive power compensation. Ultimately, both simulation results obtained were consistent with each other, thus validating the robustness of the system in maximum power extraction and reactive power compensation even under varying solar irradiance and temperature.

1. Introduction

To meet ever-increasing energy demand, it is vital to fully utilize sustainable energy sources, among which include solar PV power generation. The nature of this energy is intermittent, with efficiency of solar energy conversion to electrical energy of only 9-17% [1]. Hence, PV modules ought to be integrated with MPPT for maximum power to be generated even in adverse conditions. With the PV module placed before the DC-DC converter, selected MPPT technique would then function to control the duty cycle of the switch.

The loading of PV sources is maintained at such a level that maximum power is extracted from PV modules is done by using a DC-DC converter, specifically boost converter. Total efficiency of a PV system will be negatively affected if transferred power form PV module to network is less than optimum. Placing a boost converter in between a PV module and an inverter enables that current drawn from PV module has less ripple and is continuous [2].

Inverter placed in between the boost converter and AC grid reinverts the form of electrical power to AC and is able to provide control for the DC-link voltage and active-reactive power transfer to the grid [1]. STATCOMs are considered a member of the flexible AC transmission system (FACTS) devices. It is a shunt-connected reactive power compensation device, primarily used in AC transmission and distribution systems. Recent STATCOMs include line-commutated switches such as thyristors, which is in contrast to the basic topology of voltage source inverters (VSIs). Reactive power is exchanged with a network when the voltage source is created from a DC capacitor, whereas active power is supplied if a DC power source is connected across the capacitor. Furthermore, utilization of VSIs alongside power switches enables a closed-loop control system to control the on-off states of switches.

This allows the STATCOM to increase power quality through compensation methods such as achieving stability during transients, dynamic voltage control and oscillation damping of transmission line, in addition to active and reactive power control [3]-[12].

Preliminary STATCOM applications are based on multi-pulse converters. The multi-pulse topologies consist of six-pulse VSI circuits (otherwise known as three-level VSI). Several other self-commutated devices such as MOS-controlled thyristor (MCT), insulated gate bipolar transistor (IGBT) or integrated gate commutated thyristor (IGCT) can also be used. The gate turn-off (GTO) thyristors are switching devices which enables the converter to generate balanced three-phase AC output voltages from a DC capacitor. Adjusting the modulating frequency of GTO switches is done by varying the frequency of output voltage. An interconnection reactor is used to couple the phase voltages with the AC grid. Variations of six-pulse converters include twelve-pulse, twenty four-pulse and forty eight-pulse converters.

This paper investigated an existing MPPT algorithm for DC-DC boost converter as well as the STATCOM control scheme with sinusoidal pulse width modulation (SPWM) technique to achieve power factor correction under balanced loading condition. To verify the theoretical and practical aspects associated with the proposed STATCOM system, its average model and detailed dynamic models were presented. When compared to the average model which allows fast evaluate of system-level power and efficiency over a time interval, the detailed model gives more accurate power loss estimation by taking the transient response and harmonics into consideration, but at the cost of slower simulation speed. In order to verify all the proposed models, numerous analysis were done based on the attained results to ascertain whether the DC-link remains constant or not under two conditions: varying solar irradiation and temperature. In addition, a comparison was made between the voltage and current waveforms measured from the source-side and load-side to determine the effectiveness of the proposed models in performing reactive power compensation.

The paper is organized as follows: Section II presents the formulations of the necessary components to structure both average and detailed models. All the simulation results of the aforementioned models are reported in Section III. Finally, the conclusions are summarized in Section IV.

2. DC-DC boost inverter based STATCOM

2.1. DC-DC boost inverter

The DC-DC boost converter modelled in the detailed model is shown in Figure 1 below:

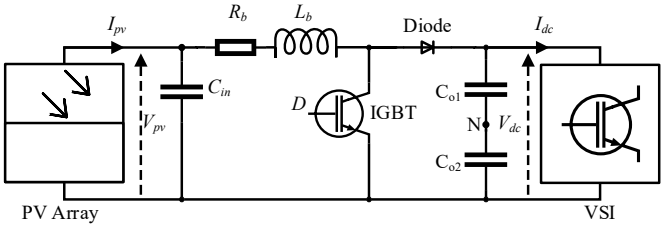

Figure 1. DC-DC boost converter (Detailed model).

Essential components that make up a boost converter is evident- an IGBT switch, a diode, an inductor (i.e., R_b and L_b), and DC capacitors (i.e., C_{o1} and C_{o2}). The duty cycle of boost converter is derived in (1) below:

$$\frac{V_{dc}}{V_{pv}} = \frac{1}{1-D} \tag{1}$$

In contrast, average model of the boost converter (see Figure 2) is designed based on (2) as follows:

$$I_{dc} = \frac{P_{pv}}{V_{dc}} = \frac{V_{pv}I_{pv}}{V_{dc}} \tag{2}$$

where V_{pv} and I_{pv} are the DC source voltage and DC source current of the boost converter from the PV array, respectively, while V_{dc} and I_{dc} define output voltage and output current generated by the boost converter, respectively.

Both average (see Figure 2) and detailed (see Figure 1) models have the following passive components in common: input capacitor C_{in}, inductor internal resistor R_b, inductor L_b, and two series-connected DC-link capacitors labelled C_{o1} and C_{o2}, respectively.

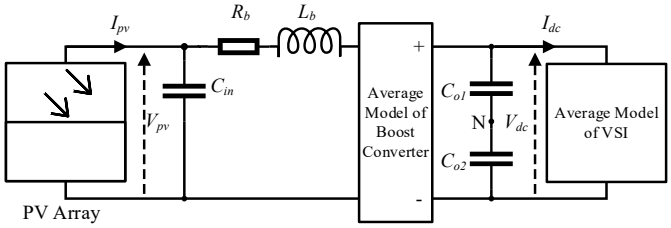

Figure 2. DC-DC boost inverter (Average model).

The inductor L_b is derived in (3) as [13]:

$$L_b = \frac{D(1-D)^2 I_{s,p-p} R_b}{\Delta I f_s} \tag{3}$$

where D is duty cycle generated via the MPPT algorithm to drive the IGBT of boost converter, $I_{s,p-p}$ is the peak-to-peak secondary-side current of the AC source transformer, ΔI is inductor ripple current, and f_s is the switching frequency of the boost converter.

The input capacitor, C_{in} is defined in (4) as [13]:

$$C_{in} = \frac{\Delta I}{8\Delta V_{pv} f_s} \tag{4}$$

where ΔV_{pv} defines the ripple voltage from the PV array.

The value of each series-connected capacitors is identical and is justified in (5) as [7]:

$$C_{o1} = C_{o2} = \frac{1}{0.001 V_o}\left[\left(\frac{1}{2}\right)\left(\frac{1}{2f_s}\right)\left(\frac{I_{s,p-p} D}{2}\right)\right] \tag{5}$$

2.2. MPPT algorithm

The flowchart depicted in Figure 3 expressed the perturb and observe (P&O) algorithm to achieve MPPT. From Figure 3, D is an output which resulted at end of each iteration of P&O algorithm starting with the measurement of PV voltage and current as follows:

$$P_{pv} = V_{pv} I_{pv} \tag{6}$$

It reads V_{pv} and I_{pv} as inputs and utilizes (6) to calculate power, P_{pv}. The power and voltage of one cycle is compared with that of the previous cycle to determine whether perturbation should be continued in a certain direction or not.

2.3. Voltage source inverter

In the detailed simulation model, the three-phase VSI operates at 50 Hz and has 3 arms of IGBT devices as shown in Figure 4. In average simulation model, an average-model based VSI is designed based on (7) as follows:

$$I_{dc} = \frac{P_{ac}}{V_{dc}} = \frac{v_{ca\_cb}(i_{ca}) - v_{bc\_cc}(i_{cc})}{V_{dc}} \tag{7}$$

When compared with detailed model, average model ensures that voltage dynamics of a system are preserved while harmonics are unpresented.

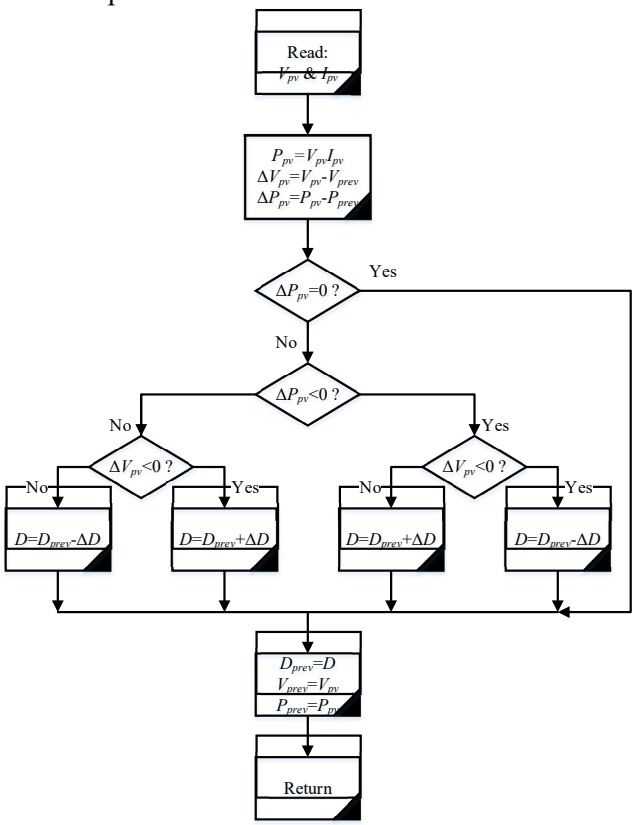

Figure 3. P&O algorithm flowchart.

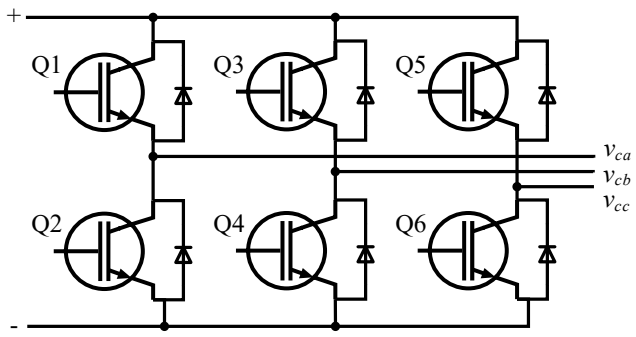

Figure 4. Schematic diagram of three-phase VSI (Detailed Model).

2.4. Control Scheme

The VSI controller for both the detailed and average models are identical as shown in Figure 5. There are two AC inputs and one DC input feeding in from the three-phase source-side (i.e., v_{sa}, v_{sb}, v_{sc} and i_{sa}, i_{sb}, i_{sc}) and the DC-link voltage, V_{dc}, respectively.

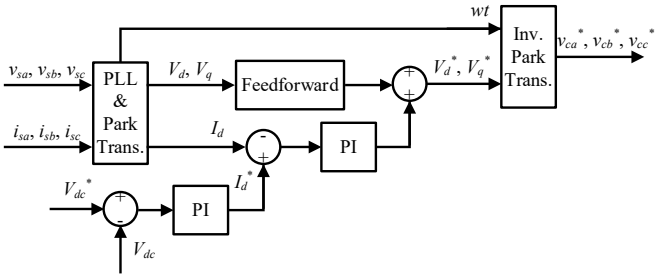

Figure 5. VSI controller (Detailed model).

From Figure 5, the phase lock loop (PLL) receives the three-phase source vectors (v_{sa}, v_{sb}, and v_{sc}) and outputted its angular angle, *wt* which is repeatedly counting between 0 to 2π at 50 Hz. The park transformation is employed to convert the vectors of any three-phase waveforms (i.e., in an *abc* reference frame) to its respective dq0 components (i.e., in a rotating reference frame). In contrast, inverse park transformation inverts any resultant dq0 back to alternating vectors as to be the modulating signals for the chosen modulation technique.

With reference to Figure 5, the voltage regulation of the boost converter is achieved via a PI controller based on the difference between the reference, V_{dc}^* and the measured, V_{dc} of DC-link voltages. It gives an output of I_d^*, which provides a current reference value for the current regulator's feedforward function as derived below [4]-[12]:

$$V_d^* = V_d - I_d R_f + I_q L_f \tag{8}$$

$$V_q^* = V_q - I_q R_f - I_d L_f \tag{9}$$

where R_f is the internal resistor of the coupling inductor, L_f.

By using inverse park transformation, (8) and (9) in rotating reference frame are inverted to the components of a three-phase system in an *abc* reference frame (i.e., v_{ca}^*, v_{cb}^*, and v_{cc}^*). The aforementioned sinusoidal components are acted as the modulating signals to be intersected with two symmetrical in-phase level-shifted triangle carriers in order to generate the respective pulse trains and drive the VSI.

The average simulation model of VSI is structured exactly similar to that of the detailed model. Instead of generating pulses as output, it requires the modulating signals only as the final outputs to be fed into the gate of average VSI model.

2.5. AC Source-side Components

The three-phase AC source-side components consist of one step-down transformer (100 kVA, 25 kV/260 V) and one $R_l L_l$ parallel load as depicted in Figure 6. These are common for both the detailed and average simulation models. From Figure 6, the secondary-side current is obtained as:

$$I_{s,p-p} = \frac{\sqrt{2}}{\sqrt{3}} \frac{S}{v_s} = \frac{\sqrt{2}}{\sqrt{3}} \frac{(P + jQ)}{v_s} \tag{10}$$

On the other hand, the parallel load has an inductive reactive power of 10 kVAR. In order to provide reactive power compensation, the VSI is connected to the point of common coupling (PCC) via the series-connected coupling impedance, $R_f L_f$. The R_f and L_f can be found with (11) and (12) as follows [4]-[12]:

$$Z_f = \sqrt{R_f^2 + X_f^2} \tag{11}$$

$$L_f = \frac{X_f}{2\pi f} \tag{12}$$

where f is the fundamental frequency of the AC source.

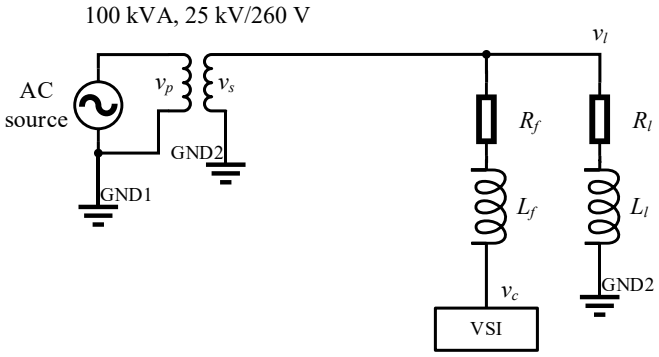

Figure 6. Single-line diagram of three-phase transmission line with STATCOM system.

3. Simulation results

The characteristic performances of both average and detailed simulation models were studied using MATLAB/Simulink software package [14]. All models were simulated with the simulation time of 5 s. Then, the effectiveness of the proposed models were demonstrated as a STATCOM system to provide reactive power compensation at the PCC as shown in Figure 7 below:

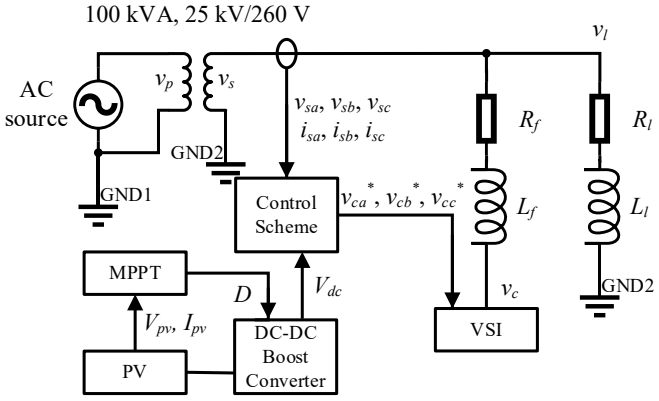

Figure 7. VSI controller (Detailed model).

The simulation studies of the proposed models were carried out with the system parameters tabulated in Table 1. Implementation of P&O in both average and detailed simulation models revealed consistent results. In designing the DC-DC boost converter, the DC-link value, V_{dc}^* of 500 V and duty cycle, D of 0.5 were assumed.

3.1. Average Model Simulation Results

To prove the robustness of the selected MPPT algorithm, the solar irradiance was ramped down to 1.25 kW/m^2 from 0.6 s to 1.1 s and the temperature was increased to 50 ºC from 2.1 s onwards (see Figure 8(a) and Figure 8(b)). At other times, the irradiance and temperature was maintained at 5 kW/m^2 and 25 ºC, respectively. Such irradiance values were chosen in view of the annual average daily irradiation in Malaysia of within 4.21 kW/m^2 to 5.56 kW/m^2 [15]. On the other hand, the temperature values of 25 ºC and 50 ºC are chosen in relation to Malaysia's tropical climate, where average temperature is approximately 27 ºC [16]-[17].

Table 1. System parameters used in the simulation study.

Parameter	Value	Unit
Grid apparent power S	100	kVA
Transformer secondary voltage v_s	260	Vrms
Transformer secondary current i_s	222	Arms
Fundamental frequency f	50	Hz
Coupling inductor L_f	1.00427	mH
Internal resistor of R_f	0.03155	Ω
Load power factor	0.8	
Switching frequency f_s	5	kHz
PV array ripple voltage ΔV_{pv}	0.0273	
Inductor ripple current ΔI	0.1	
Inductor L_b	4.71	mH
Inductor internal resistance R_b	0.005	Ω
Input capacitor C_{in}	91.58	μF
Output capacitor C_{o1}	7850	μF
Output capacitor C_{o2}	7850	μF

Figure 8 demonstrated that in consideration for the variation of solar irradiance and temperature, utilization of P&O based MPPT to drive the boost converter could ensure attaining constant DC-link voltage, V_{dc} (i.e., the output voltage of boost converter shown in Figure 8(e)) throughout the simulation period.

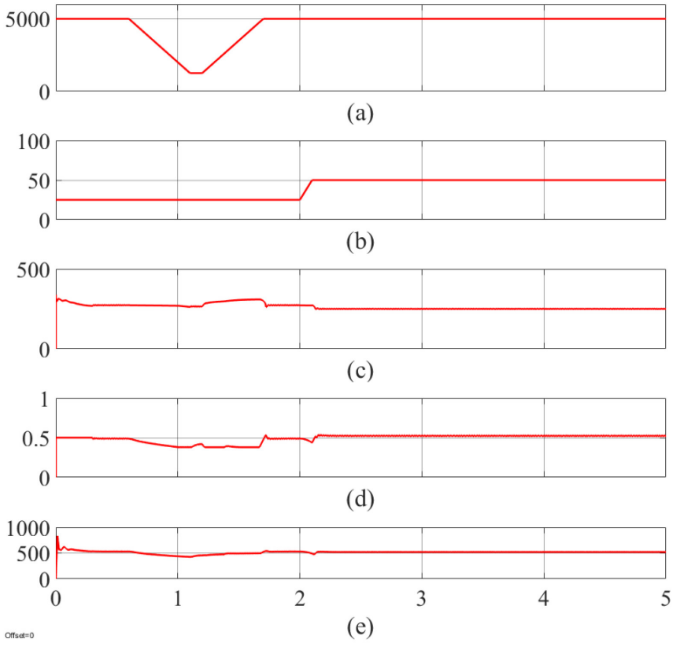

Figure 8. Average model of (a) solar irradiance, (b) temperature (c) PV voltage V_{pv}, (d) duty cycle D, and (e) DC-link voltage V_{dc}.

Figure 9 and 10 depicted the AC voltage and AC current waveforms at the load-side and source-side (i.e., primary side of the transformer), respectively, to investigate the occurrence of reactive power compensation. Particularly, Figure 9 showed that the load current, i_l was phase-lagging with respect to

the load voltage, v_l by 37º; indicating the non-unity power factor operation in electricity generation if there is no STATCOM connected to the PCC.

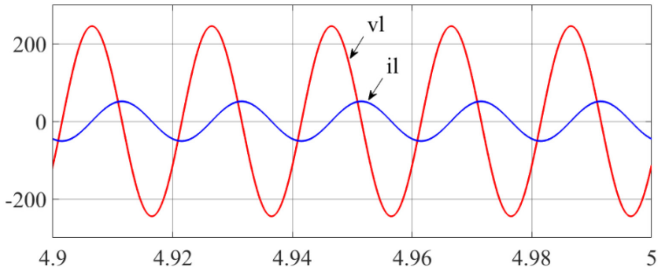

Figure 9. Average model of load voltage v_l and load current i_l.

With STATCOM system, Figure 10 demonstrated that both the AC source voltage, v_p (i.e., after scaled down by 1000) and AC source current, i_p were in-phase; indicating the effectiveness of the proposed model to provide power factor correction.

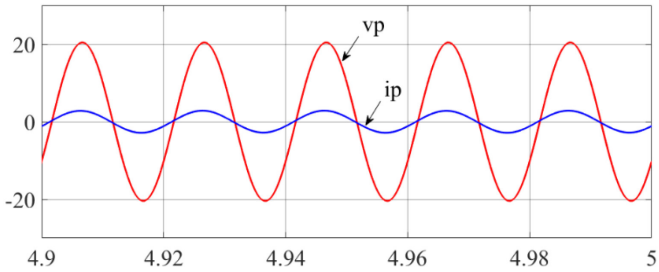

Figure 10. Average model of primary AC source voltage v_p and primary AC source current i_p.

Moreover, with unity power factor operation, Figure 10 illustrated the amplitude of AC source current, i_p was significantly lower when compared with Figure 9 as it required to generate active power only.

3.2. Detailed model simulation results

The detailed model was simulated with similar simulation period (i.e., 5 s) to validate the results attained from average model. The significance of this work lies in the successful implementation of the selected MPPT algorithm (P&O) and the STATCOM control scheme (d-q theory). This is proven from the consistent results obtained from both average and detailed simulation models (see Table 2 and Figure 11).

Table 2 is a tabulation of the steady-state values obtained from both models for comparison. While the simulation results for both models show that the duty cycles remained within 0.5 (see Figure 8(d) for average model and Figure 11(d) for detailed model), the DC-link voltage, V_{dc} was increased to a value close to 525 V (see Figure 11(e)). The increase in DC-link voltage, V_{dc} from the previously assumed value of 500 V used in designing the converter could be inferred from the decrease in simulated PV voltage, V_{pv} obtained of only close to 250 V instead of the assumed 273 V.

Table 2. System parameters used in the simulation study.

Parameters	Average Model	Detailed Model	Unit
PV voltage V_{pv}	250.00	250.80	V
DC-link voltage V_{dc}	525.11	525.79	V
Duty cycle	0.5195	0.5255	
VSI voltage v_c	368.50	377.60	V_{peak}
VSI current i_c	282.90	264.30	A_{peak}

Parameters	Average Model	Detailed Model	Unit
Primary source-side voltage v_p	2.041	2.041	kV_{rms}
Primary source-side current i_p	2.878	2.756	A_{rms}

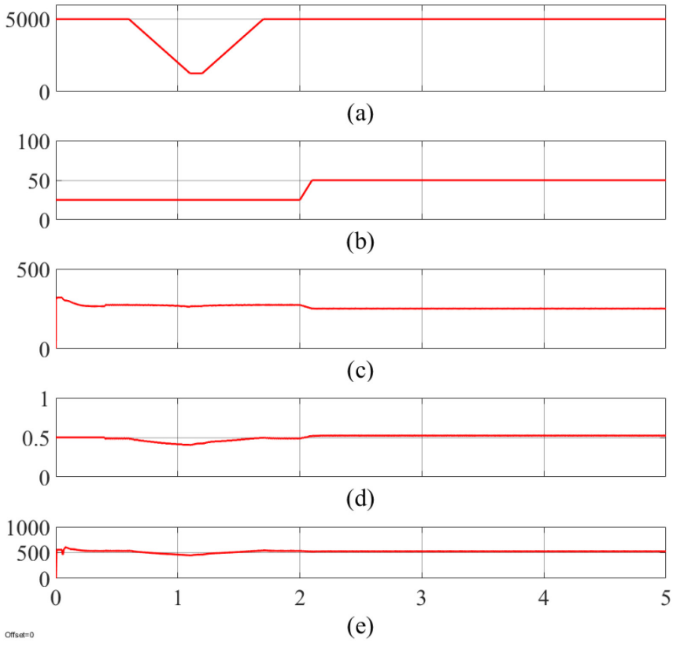

Figure 11. Detailed model of (a) solar irradiance, (b) temperature (c) PV voltage V_{pv}, (d) duty cycle D, and (e) DC-link voltage V_{dc}.

Figure 12 and Figure 13 illustrated the before and after the STATCOM system connected at the PCC, respectively. Once again, the proposed model demonstrated its capability to ensure unity power factor operation in generating and transmitting electricity (see Figure 13).

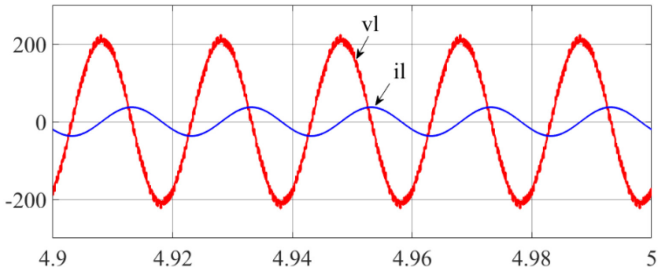

Figure 12. Detailed model of load voltage v_l and load current i_l

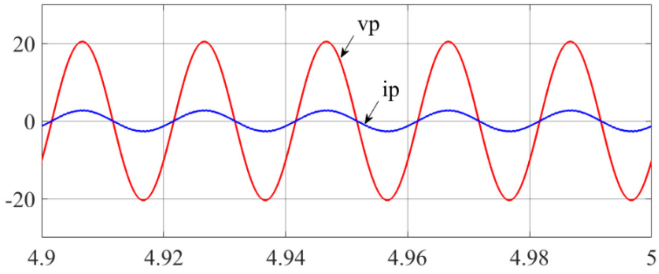

Figure 13. Detailed model of primary AC source voltage v_p and primary AC source current i_p.

Figure 14 illustrated the input power, P_{pv} and the AC source power, P_p from the primary side of the transformer. By referring back to Figure 11(a), both the aforementioned power parameters tracked the

trend of the varying solar irradiance. This is evidence to the fact that maximum power is extracted even at low irradiance.

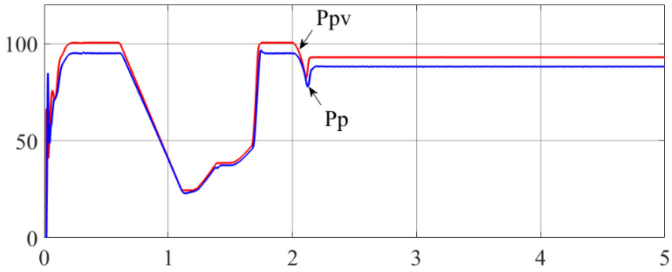

Figure 14. Average model of PV power P_{pv} and primary source power P_p.

4. Conclusions

In conforming to the Malaysian transmission network of 132 kV, the AC source-side generator was set to a value of 132 kV accordingly. Evidently, this paper was designed to suit the needs of Malaysia, particularly in terms of climate and existing transmission network. Upon investigating the conventional and hybrid approaches to both MPPT algorithms and STATCOM control schemes, the P&O MPPT algorithm and d-q STATCOM control scheme were chosen to be implemented. To accommodate the energy needs in Malaysia, solar irradiance of 1.25 kW/m^2 and 5 kW/m^2, as well as temperature of 25°C and 50°C was applied with regards to the simulations conducted. The purpose of this work was fulfilled in the successful attainment of maximum power from PV and occurrence of reactive power compensation; both of which were due to the appropriate implementation of selected MPPT algorithm and STATCOM control scheme. An average simulation model was first designed and implemented. To verify the results obtained, a second detailed simulation model was designed and simulated. Both models had parameters that were exactly similar, except that the detailed model exhibited harmonics. In addition, both power factor values were corrected to unity after compensation.

5. References

[1] A. Maiti, K. Mukherjee, and P. Syam, "Design, modeling and software implementation of a current-perturbed maximum power point tracking control in a DC-DC boost converter for grid-connected solar photovoltaic applications," Int. Conf. on Control, Meas. and Instrum., 2016, pp. 36-41.

[2] H. Toodeji, N. Farokhnia, and G. H. Riahy, "Integration of PV module and STATCOM to extract maximum power from PV," Int. Conf. on Electr. Power and Energy Convers. Syst., 2009, pp. 1-6.

[3] S. R. Farhad Shahnia, Arindam Ghosh, Static Compensators (STATCOMs) in Power Systems. Singapore Springer, 2015.

[4] K. H. Law, M. S. A. Dahidah, and N. Mariun, "Cascaded Multilevel Inverter based STATCOM with Power Factor Correction Feature," IEEE Conf. on Sustain. Utilization and Develop. in Eng. And Technol., pp. 1-7, 2011.

[5] K. H. Law, M. S. A. Dahidah, and H. A. F. Almurib, "SHE–PWM Cascaded Multilevel Inverter With Adjustable DC Voltage Levels Control for STATCOM Applications," IEEE Trans. Power Electron., vol. 29, no. 12, pp. 6433-6444, 2014.

[6] K. H. Law, M. S. A. Dahidah, G. S. Konstantinou, and V. G. Agelidis, "SHE–PWM Cascaded Multilevel Inverter With Adjustable DC Voltage Levels Control for STATCOM Applications", Int. Conf. on Power Electron. And Motion Cont., pp. 330-334, 2012.

[7] K. H. Law and M. S. A. Dahidah, "DC-DC Boost Converter based MSHE-PWM Cascaded Multilevel Inverter Control for STATCOM Systems", Int. Conf. on Power Electron., pp. 1283-1290, 2014.

[8] K. H. Law and M. S. A. Dahidah, “New Current Control Algorithm Incorporating Multilevel SHE-PWM Approach for STATCOM Operation Under Unbalanced Condition,” Int. Symp. Power Electron. for Distrib. Generation Syst., pp. 1-7, 2014.
[9] K. H. Law, M. S. A. Dahidah, and H. A. F. Almurib, “A New Reactive Current Reference Algorithm for the STATCOM System Based on Cascaded Multilevel Inverters,” IEEE Trans. Power Electron., vol. 30, no. 7, pp. 3577-3588, 2015.
[10] J. S. X. Ong, K. S. K. Yong, K. H. Law, W. P. Q. Ng, and M. Dahidah, “CCM and DCM analysis of quasi-z-source inverter,” IEEE Conf. Energy Conversion, DOI: 10.1109/CENCON.2017.8262476.
[11] K. H. Law, “An Effective Voltage Controller for Quasi Z-Source Inverter based STATCOM with Constant DC-Link Voltage”, IEEE Trans. Power. Electron., DOI: 10.1109/TPEL.2017.2772309, pp. 1-13.
[12] K. H. Law, W. P. Q. Ng, W. K. Wong, “Flyback cascaded multilevel inverter based SHE-PWM control for STATCOM applications,” Int. J. of Power Electron. and Drive Syst., vol. 8, no. 1, pp. 31-38, 2017.
[13] A. Vangari, D. Haribabu, and J. N. Sakamuri, "Modeling and control of DC/DC boost converter using K-factor control for MPPT of solar PV system," Int. Conf. on Energy Economics and Environment, pp. 1-6, 2015.
[14] MathWorks. (1994–2018). [Online]. Available: http://www.mathworks.com/
[15] S. Mekhilef, M. Barimani, A. Safari, and Z. Salam, "Malaysia’s renewable energy policies and programs with green aspects," Renewable and Sustainable Energy Reviews, vol. 40, pp. 497-504, 12// 2014.
[16] N. I. Ahmad, M. Z. A. Kadir, M. Izadi, N. H. Zaini, M. A. M. Radzi, and N. Azis, "Effect of temperature on a poly-crystalline solar panel in large scale solar plants in Malaysia," Conf. on Energy Convers., pp. 244-248, 2015.
[17] K. H. Law. S. K. Yong, W. P. Q. Ng, M. Dahidah, "Lead compensator design for single-phase quasi z-source inverter," J. of Telecommunication, Electron. and Comput. Eng., vol. 10, no. 1-12, pp. 39-44, 2018.